DEVELOPMENT OF A ROBOTIC END-EFFECTOR FOR APPLE TREE PRUNING

A. Zahid, L. He, L. Zeng, D. Choi, J. Schupp, P. Heinemann

ASABE Research

HIGHLIGHTS

- An end-effector with two degrees of freedom (2R) was developed for pruning apple trees.
- A rational 2×2 relationship ($R^2 = 0.93$) was found for 'Fuji' apple tree branch diameter and cutting force.
- Simulation showed that the cutter can be aligned in a wide range of orientations in a spherical workspace.
- The developed end-effector was able to cut branches up to 12 mm in diameter.

ABSTRACT. *Robotics and automation technologies are now used extensively in agriculture, while production operations for tree fruit crops still largely depend on manual labor. Manual pruning is a labor-intensive and costly task in apple production. Robotic pruning is a potential solution, but it involves several challenges due to the unstructured work environment. This study focused on designing an end-effector prototype for pruning considering the maneuvering, spatial, mechanical, and horticultural requirements. Branch cutting force was measured with a thin force sensor to provide guidelines for the end-effector design. The test results indicated the relationship between the force required to cut different diameter branches with an R^2 value of 0.93. The end-effector was developed using two rotary motors, a pneumatic cylinder, and a pair of bypass shear blades. A three-directional linear manipulator system and a control system were built for moving the end-effector to targeted locations. A mathematical model was developed for simulation of the workspace utilization and reachable points of the end-effector. The simulation results indicated that the end-effector can be aligned in a wide range of orientations of the cutter. Field tests were conducted for validation of the simulation results and performance assessment of the end-effector. The results indicated that the end-effector with the current parameter settings successfully cut branches up to 12 mm in diameter and was able to cut branches in a wide range of possible orientations in a given 3D space. The robotic end-effector developed in this study is a core component of an automated pruning system for fruit trees. In future work, an integrated manipulator system will be developed for branch accessibility with collision-free trajectories.*

Keywords. Malus × domestica *(Borkh.), Pruning end-effector, Reachable-points simulation, Tree pruning.*

In the U.S., the tree fruit industry contributes one-fourth ($18 billion) of all specialty crop production, and apples represent one of the most valuable non-citrus fruits (USDA-NASS, 2018). Pruning is a cultivation technique that affects fruit quality and quantity as well as the efficacy of pest control practices (Glenn and Campostrini, 2011; Mercier et al., 2008). Mechanization and automation have been successfully implemented in row crops; however, production operations for specialty crops such as tree fruits still largely depend on manual labor (Silwal, 2016). Mika et al. (2016) stated that 80 to 120 working hours of skilled labor are required per hectare for manual pruning of peach, pear, and apple trees. Gallardo et al. (2009) estimated that pruning of apple trees comprises 20% of the total pre-harvest production cost. Conventional manual pruning complicates the sustainability of the tree fruit industry due to increasing labor costs and the limited labor pool. To address these issues, this research focuses on automated mechanical pruning.

Recently, robotic systems have been studied for automated operations in tree fruit crops, mainly for fruit harvesting. Robotic fruit harvesting systems were reviewed by Bac et al. (2014). Those systems used cameras to identify fruits and directed the robotic end-effector accordingly, but the accuracy for spotting fruits was reported to be low (Zhang et al., 2011; Li et al., 2011). Their success was limited due to challenges such as the natural variability in tree architectures (Bac et al., 2014; Kapach et al., 2012; Li et al., 2011). Although researchers have reported image acquisition systems for 3D reconstruction of branches (Karkee et al., 2014; Lindner et al., 2007; Nakarmi and Tang, 2012), only a few studies have reported the use of robotic end-effectors for fruit tree pruning (Bac et al., 2014; He and Schupp, 2018; Kondo et al., 1993, 1994).

Submitted for review in October 2019 as manuscript number MS 13729; approved for publication as a Research Article by the Machinery Systems Community of ASABE in April 2020.

The authors are **Azlan Zahid,** Doctoral Student, and **Long He,** Assistant Professor, Department of Agricultural and Biological Engineering, The Pennsylvania State University; **Lihua Zeng,** Visiting Scholar, Department of Agricultural and Biological Engineering, The Pennsylvania State University, and Associate Professor, College of Engineering, Hebei Agriculture University, Baoding, China; **Daeun Choi,** Assistant Professor, Department of Agricultural and Biological Engineering, **James Schupp,** Professor, Department of Plant Science, and **Paul Heinemann,** Professor and Head, Department of Agricultural and Biological Engineering, The Pennsylvania State University, State College, Pennsylvania. **Corresponding author:** Long He, Fruit Research and Extension Center, 290 University Drive, Biglerville, PA 17307; phone: 717-677-6116; e-mail: luh378@psu.edu.

  ISSN 2151-0032 https://doi.org/10.13031/trans.13729

Robotic pruning, which is selective pruning with accurate cuts, typically cuts the branches with an end-effector consisting of a cutting blade and anvil that use a scissors motion (Lehnert, 2012). In the 1990s, a manipulator and vision system was developed for multi-purpose vineyard pruning (Kondo et al., 1993). More recently, a prototype was developed for spur pruning of grapevines using a stereo camera and robotic end-effector (Vision Robotics, 2015). That system did not require 3D reconstruction of the branches and worked with pre-specified targets, so collision avoidance was unnecessary. The target points were easy to reach, and a simple point-to-point path was used for controlling the trajectory of the robotic arm. However, those studies focused on grapevines, which have simple and uniform architectures (He and Schupp, 2018).

In a robotic system, an effective end-effector is a core component for performing the desired task. As mentioned earlier, few robotic end-effectors have been developed specifically for branch pruning. In the past, robotic end-effectors with saw-type cutters have been investigated for fruit harvesting. A disc cutter end-effector with an eye-in-hand configuration was developed by Dong and Zhu (2015). The tool was integrated with a 6 DoF arm to control the orientation and gripping function of the end-effector. Similarly, a belt-driven saw-type end-effector integrated with a 3 DoF dual arm for tomato harvesting was developed by Zhao et al. (2016), with a tool that was able to move within a range of -45° to 45° along the *x*-axis. Jeon and Tian (2009) developed an end-effector with continuous-motion cutter blade mechanisms for weed cutting and direct chemical application. Those studies used disc-type cutters, which cannot produce the smooth cut essential for fruit tree pruning. Those studies also did not consider the spatial requirements of the end-effector.

Some studies have reported the use of shear blades for end-effector design. Feng et al. (2018) developed a robotic end-effector using shear blades for harvesting tomatoes. Their end-effector used a pneumatic cylinder for opening and closing the cutters. Ling et al. (2004) developed a robotic end-effector for harvesting tomatoes using a 20 cm (8 in.) linear-motion actuator for controlling the movement of a cutter and vacuum cup. In a recent study, an end-effector was designed for eggplants using a central linear-motion actuator to control the cutting mechanism (Hui et al., 2018). Although those end-effectors with linear actuators performed well, the force produced by the linear actuator was not enough to cut tree branches, and the size of the linear actuator was not appropriate considering the complex architecture of fruit trees. Tree pruning requires a large force, which can be achieved by powerful actuators, but the application of such end-effectors in tree branch pruning is limited by spatial requirements.

Robotic pruning of apple trees is challenging because of their complex canopy architecture. The branches may be crowded and overlapped, with very little space available for the robot to interact with branches. Therefore, designing an end-effector for fruit tree pruning requires many considerations, including spatial and horticultural requirements and maneuverability of the tool within the canopy. Kondo and Ting (1998) stated that the design characteristics and mechanism of an end-effector depend on the task being performed. The end-effector design should consider the physical, mechanical, and biological properties, including shape, size, weight, cutting resistance, and maneuverability based on the intended task. An end-effector designed for specific properties is not suitable for multipurpose use but rather for specific use to achieve efficient operation. Botterill et al. (2017) developed an end-effector with a CNC router mill-end cutter for pruning grapevines; however, the cutter failed to make complete cuts due to the long motion required to cut the canes. In addition, the spatial requirements of the cutter were not considered in the design, which limited its access to the targeted canes without colliding with other canes.

A compact end-effector is essential to reach pruning points close to the tree trunk. Huang et al. (2016) presented design requirements for pruning end-effectors, including spatial and mechanical considerations. The end-effector should be maneuverable with minimal spatial requirements by a robotic arm to reach the targeted position following a collision-free path. The trajectory is critical, and collision avoidance is required for robotic tree pruning. The mechanical and dynamic performance of the end-effector largely depends on the spatial considerations, which affect the weight, size, and orientation of the end-effector. Because the end-effector is attached to a robotic arm, it must correlate with the bearing capacity of the arm (Huang et al., 2016). Moreover, the horticultural requirements for a pruner end-effector are also critical. The end-effector should be able to produce a smooth cut because rough cuts can cause rot and affect the healing process. The end-effector should also be able to align within the allowable cutting angle range to produce square or bevel cuts based on the branch collar and bark ridge to prevent water or snow damage. Another important consideration for tree pruning is the need for selective pruning. The complete cycle of selective pruning includes branch identification, tool positioning, and the cutting process. The design of an effective pruning end-effector should be well-suited for all these processes.

The primary goal of this study was to develop an effective end-effector capable of generating sufficient force for apple tree pruning, considering the maneuverability, spatial requirements, and mechanical interactions of the end-effector, to cut branches at any orientation in tall spindle tree architecture. The specific objectives of this study were to measure the force required for branch pruning (design parameter), design a pruning end-effector, and evaluate the performance of the designed end-effector in field conditions. The study also involved the development of a mathematical model to simulate the end effector workspace and cutter orientation in 3D space.

Material and Methods

Pruning Force and Torque Measurement

The amount of force required to cut tree branches is an important parameter for end-effector design. The force measurement was performed using a manual pruner and a flexible and ultra-thin force sensor (Phidgets-1131, Phidgets Inc., Calgary, Alberta, Canada). This sensor has the capacity

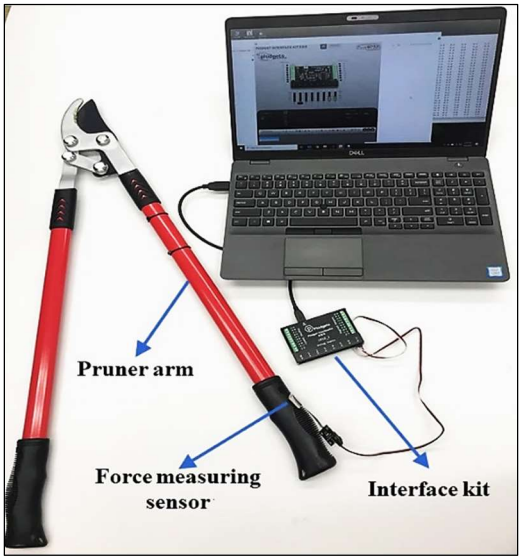

Figure 1. Manual pruner equipped with sensor for force measurement.

to measure 2 kg of force. The sensor was attached to the arm of the manual pruner (fig. 1) and positioned to coincide with the point of contact of an operator's finger with the handle to measure the force applied during pruning. The distance between the sensor and the cutter pivot was 60 cm. The cutting torque was calculated using the measured force and the length of the pruner arm. For design of the end-effector, the torque was converted to the end-effector force according to the dimensions of the end-effector. The measurement tests were conducted in the laboratory. Ten primary branches with secondary branches were selected randomly from five 'Fuji' apple trees, and 75 cuts were made on ten branches of different diameters. The branch diameter and applied force were recorded during the tests and used for calculating the torque required to cut branches of different diameters. The maximum force for each finger impression was used to establish the relationship between the amount of torque required and the corresponding branch diameter.

Robotic End-Effector Development

End-Effector Design

The architecture of apple trees is complex, and the branches have different diameters and orientations. When designing a pruning end-effector, it is important to consider the spatial requirements as well as flexibility of the pruning orientation. A concept design of the robotic end-effector in SolidWorks (v.2019, Dassault Systèmes, Vélizy-Villacoublay, France) is shown in figure 2. The cutter consists of a cutting blade and an anvil. The anvil is fixed to the frame, and the blade is attached to a pneumatic cylinder, which is fixed in-line with the anvil on the same L-shaped frame. The pneumatic cylinder is normally in its extended position, and a cut is performed when the cylinder is retracted. Considering the required maneuverability of the end-effector, the concept design includes two angular movements: one using the main motor (M1), and the other using the orientation motor (M2). The end-effector is attached to the orientation motor, which is then attached to the main motor. The main motor and orientation motor can rotate 360° in both clockwise and counterclockwise directions. The combination of M1 and M2 allows the end-effector to align the cutter perpendicularly with a tree branch at any orientation.

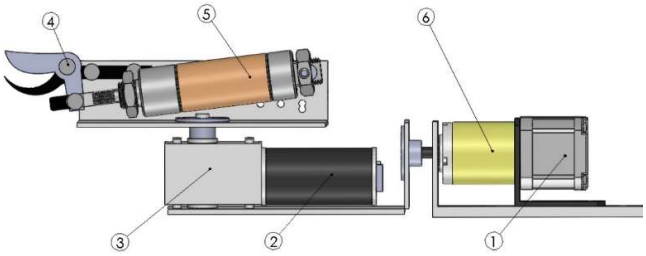

Figure 2. Concept design of end-effector: (1) main motor (M1), (2) orientation motor (M2), (3) self-locking worm gearbox, (4) pruner, (5) pneumatic actuator, and (6) planetary gearbox.

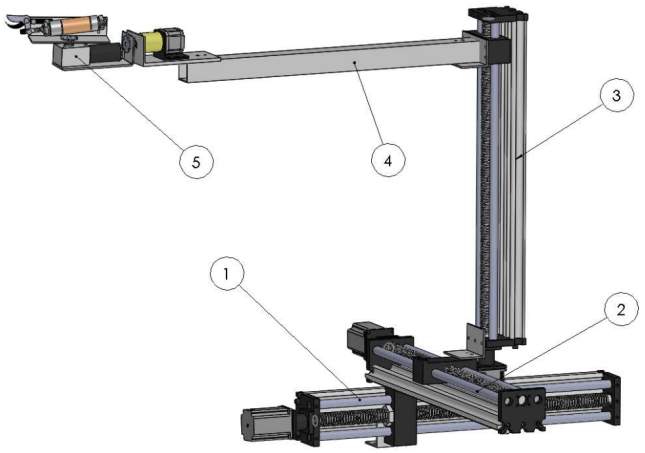

Figure 3. Concept design of end-effector attached to manipulator with three linear actuators: (1) linear actuator L1, (2) linear actuator L2, (3) linear actuator L3, (4) linear arm, and (5) end-effector.

After the design of the end-effector, a three-directional linear manipulator was designed as a base platform to move the end-effector to the targeted locations in a given 3D space. The 3D model of the proposed platform was designed in SolidWorks, as shown in figure 3. The movements of the three linear actuators (L1, L2, and L3) are independent of each other in three directions. Actuator L1 provides the base motion of the actuator system, while L2 is attached to the slider of L1, and L3 is attached to the slider of L2. One end of a linear arm is attached to the slider of L3, and the end-effector is mounted on the other end.

End-Effector Assembly

With the concept designs of the end-effector and the three directional manipulators, the robotic end-effector system was assembled as shown in figure 4. The main components of the system included stepper motors, the bypass shear blade pruner, the pneumatic cylinder, and the linear motion actuators. The specifications are given in table 1. The components were selected based on the data recorded in the pruning force measurement tests. The end-effector was developed using two motors and one pneumatic cylinder (fig. 4b).

Motor M1 was a NEMA 17 stepper motor with a 51:1 planetary gearbox. Motor M2 was a 108:1 self-locking worm gearbox motor for high holding torque. M1 was mounted directly

(a) (b)

Figure 4. Robotic pruning system: (a) integration of end-effector with three linear actuators and (b) end-effector in use.

Table 1. Specifications of components used in this study.

Item	Model or Type	Quantity	Specifications
Main motor	Stepper NEMA 17	1	0.035° per step, 4 N·m holding torque, 1.68 A, 24 VDC, 51:1 gear ratio
Orientation motor	Worm gear motor	1	74 rpm no-load speed, 25 kg·cm torque, 24 VDC, 108:1 gear ratio
Stepper driver/controller	Bipolar	4	1.0 to 4.2 A, 20 to 50 VDC, microstep (400 to 25,600 steps per rev.)
Pneumatic cylinders	Single-acting	1[a]	2.5 cm bore, 2.54 cm stroke, 60 kg force at 103 N cm^{-2} 2.2 cm bore, 2.54 cm stroke, 27 kg force at 103 N cm^{-2}
Linear motion actuators	Slider	3	60 and 50 cm travel, 1.8 NM 57 stepper motor, 3 A, 24 VDC
Relays	Sun founder	1	Four-channel relay module, normally open
Solenoid valve	MME-31PES-D012	1	Two-position, three-way
Limit switches	SN04-N	3	10 to 30 VDC, NPN

[a] Two different pneumatic cylinders were used to provide different cutting forces.

on the robotic arm using a standard NEMA 17 mounting bracket. The 5 cm wide L-shaped mounting frame for M2 had a base length of 26 cm and the smaller side, where the shaft of M1 was fixed, had a height of 5 cm. The L-shaped frame for the pruning mechanism had a width and height of 5 cm × 5 cm and a length of 21 cm. The shaft of M2 was fixed at the bottom center of this frame using a flange coupling. The attachment of the pruner to the end-effector was critical. A commercial pruner replacement blade was used for the end-effector. The stationary part of the pruner was attached to the L-shaped frame. Opening and closing of the pruner blade were controlled with a single-acting pneumatic cylinder. Two different pneumatic cylinders, with 2.2 and 2.54 cm bore diameters, were used to provide different cutting forces. The travel length was 50 cm for linear actuators L1 and L2 and 60 cm for linear actuator L3.

End-Effector Control System

A microcontroller (Arduino Mega 2560) was used to control the robotic end-effector and the linear manipulator (fig. 5). All stepper motors were driven by motor drivers to control their speed and rotation. The orientation motor (M2) was a DC motor, and two relays were used for directional control. Another relay was used to control the solenoid valve to retract and release the pneumatic cylinder. A MATLAB-based

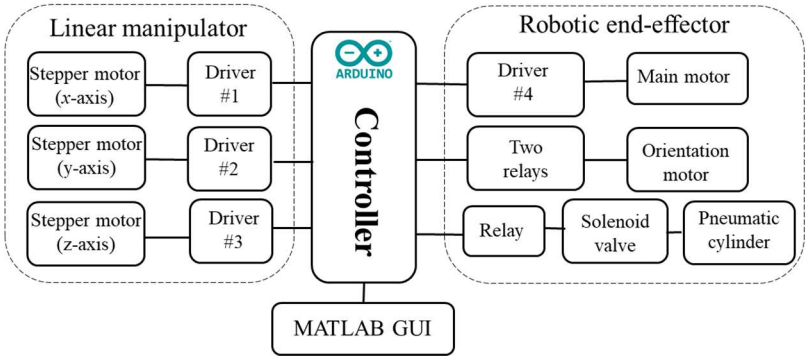

Figure 5. Control system for robotic end-effector.

graphical user interface (GUI) was created for the control system. The location of the end-effector can be set through the GUI to control the movement of the three stepper motors in the linear manipulator. The angles of the main motor and orientation motor in the end-effector can also be set through the GUI to change the orientation of the cutter.

A three-step process was designed to control the branch cutting operation of the robotic end-effector. The first step was to position the end-effector. For operation of the three linear actuators, the distances were entered manually through the GUI to move the end-effector to the targeted position. The movements of the linear actuators can occur separately or simultaneously. The second step was to align the cutter perpendicular to the target branch. To align the cutter, the angles for motors M1 and M2 were entered manually through the GUI. The third step was to cut the target branch by retracting the pneumatic cylinder, which was controlled by energizing the solenoid valve through the GUI. The same cycle was repeated for the next branch. Currently, the cutting process is performed manually because the coordinates of the target location for the end-effector are estimated. Therefore, multiple attempts may be needed to move the end-effector to the precise location and orientation with the three linear actuators (L1 to L3) and two motors (M1 and M2).

END-EFFECTOR WORKSPACE SIMULATION

Simulation for tracking the cutter end point and the orientation of the cutter at different reachable points was performed using a homogeneous transformation matrix. Coordinate frames were defined to obtain the desired matrix for representing the rotations and transformations. The first vector frame was the base (reference) frame and was defined as global coordinates, i.e., $O(x_0, y_0, z_0)$. The first rotational vector frame was defined at the starting point of link 1, i.e., $P_1(x_1, y_1, z_1)$, and the second rotational frame was defined for link 2, i.e., $P_2(x_2, y_2, z_2)$, for the rotation of motors M1 and M2, i.e., θ_1 and θ_2, respectively. The last frame was defined at the position of the cutter, i.e., $P_3(x_3, y_3, z_3)$, to determine the orientation at each reachable point. An illustration of the mechanism is shown in figure 6.

The transformation matrix and position vector matrix (Spong et al., 2006) for the developed end-effector are given as:

$$ {}^{i-1}_{i}T = \begin{bmatrix} {}^{i-1}_{i}\mathrm{Rot} & {}^{i-1}p_i \\ 0^T & 1 \end{bmatrix} \tag{1} $$

$$ {}^{i-1}_{0}p_i = \begin{bmatrix} d_{xi} & d_{yi} & d_{zi} \end{bmatrix}^T \tag{2} $$

where I = 1, 2, 3; ${}^{i-1}_{i}T$ is the representation of the transformation matrix; ${}^{i-1}_{i}\mathrm{Rot}$ is the rotation matrix of the individual coordinate frame; ${}^{i-1}p_i$ is the translational vector corresponding to the previous coordinate frame; and d_{xi}, d_{yi}, and d_{zi} are the coordinates of individual vector frames in the x, y, and z directions, respectively. Based on the mechanism and defined coordinate systems shown in figure 6, the rotation matrices and position vectors for two neighboring coordinate systems are given as equations 3 to 8:

$$ {}^{0}_{1}\mathrm{Rot} = \begin{bmatrix} 1 & 0 & 0 \\ 0 & 1 & 0 \\ 0 & 0 & 1 \end{bmatrix} \tag{3} $$

$$ {}^{0}p_1 = \begin{bmatrix} a_1 & 0 & 0 \end{bmatrix}^T \tag{4} $$

$$ {}^{1}_{2}\mathrm{Rot} = \begin{bmatrix} 1 & 0 & 0 \\ 0 & \cos\theta_1 & -\sin\theta_1 \\ 0 & \sin\theta_1 & \cos\theta_1 \end{bmatrix} \tag{5} $$

$$ {}^{1}p_2 = \begin{bmatrix} b_1 & 0 & b_2 \end{bmatrix}^T \tag{6} $$

$$ {}^{2}_{3}\mathrm{Rot} = \begin{bmatrix} \cos\theta_2 & -\sin\theta_2 & 0 \\ \sin\theta_2 & \cos\theta_2 & 0 \\ 0 & 0 & 1 \end{bmatrix} \tag{7} $$

$$ {}^{2}p_3 = \begin{bmatrix} c_1 & 0 & 0 \end{bmatrix}^T \tag{8} $$

where a_1 is the fixed base length of the end effecter along the x-axis, b_1 and b_2 are the length and height of link 1 (mounting body) along the x-axis and z-axis, respectively, c_1 is the length of link 2 (orientation body) along the x-axis, and θ_1 and θ_2 are the rotation angles of motors M1 and M2, respectively. The cutter (end point) position and orientation were calculated using the homogenous transformation matrix. The first three expressions in the last column of equation 9 return

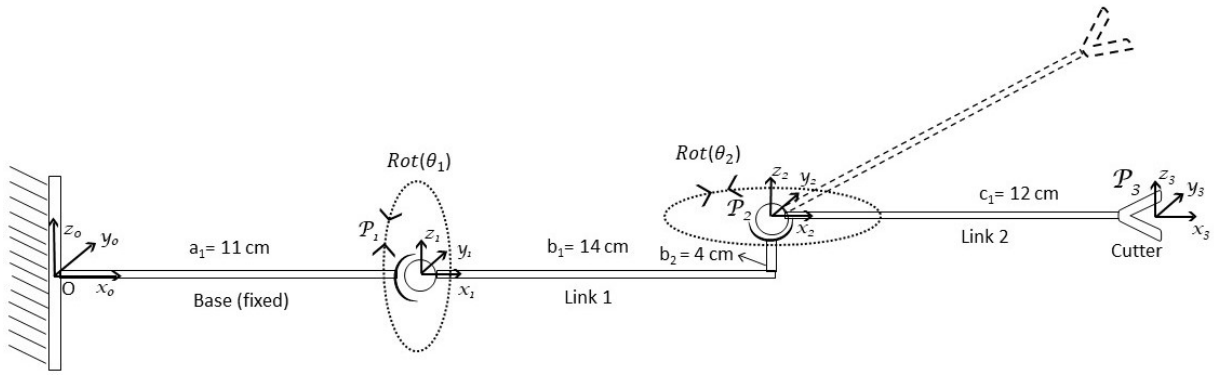

Figure 6. Illustration of end-effector mechanism.

the position of the cutter end point, i.e., x_3, y_3, and z_3 in reference coordinates, with the expression given as:

$$ {}^{0}_{3}T = {}^{0}_{1}T\,{}^{1}_{2}T\,{}^{2}_{3}T = $$

$$ \begin{bmatrix} \cos\theta_2 & -\sin\theta_2 & 0 & a_1 + b_1 + c_1\cos\theta_2 \\ \cos\theta_1\sin\theta_2 & \cos\theta_1\cos\theta_2 & -\sin\theta_1 & -b_2\sin\theta_1 + c_1\cos\theta_1\sin\theta_2 \\ \sin\theta_1\sin\theta_2 & \cos\theta_2\sin\theta_1 & \cos\theta_1 & b_2\cos\theta_1 + c_1\sin\theta_1\sin\theta_2 \\ 0 & 0 & 0 & 1 \end{bmatrix} \quad (9) $$

The coordinates of the cutter in the global coordinate system are:

$$ P_x = a_1 + b_1 + c_1\cos\theta_2 \quad (10) $$

$$ P_y = -b_2\sin\theta_1 + c_1\cos\theta_1\sin\theta_2 \quad (11) $$

$$ P_z = b_2\cos\theta_1 + c_1\sin\theta_1\sin\theta_2 \quad (12) $$

where P_x, P_y, and P_z are the coordinate values of the cutter in the global coordinate system in the x, y, and z directions, respectively.

To simulate all the reachable points, the rotation (θ_1 and θ_2) was iterated in loops to implement a direct geometry approach to consider all possible points reachable by the end-effector. Because it was not possible to run a continuous simulation, as the number of reachable points using direct geometry is indefinite, a discretization method was used to reduce the number of points in the simulation. The simulation was conducted in MATLAB (ver. 2019a, MathWorks, Natick, Mass.). A 20° step angle function for both θ_1 and θ_2 was created to discretize the range of values between 0° and 360° for each motor. For plotting of the cutter frame at all the simulated points, a function was created to reduce the number of cutter frames in the workspace graph for the given simulated points. The reduced number of cutter frames was plotted to cover the entire workspace of the end-effector. When all the simulated points were obtained, another loop was used to iterate the points matrix and plot the results on the graph.

End-Effector Field Evaluation

The developed end-effector was intended for use in modern high-density tree architectures, including tall spindle, V-trellis, and fruiting wall structures. These training systems have no permanent branches, and most of the branches are accessible from outside the canopy. The diameter of the pruned branches is usually less than 15 to 20 mm. The smaller and fewer branches, as compared to conventional tree structures, make high-density tree structures feasible for robotic applications. For this study, the field test for validation of the simulation results and performance assessment of the end-effector was conducted on tall spindle 'Fuji' apple trees at the Penn State Fruit Research and Extension Center (FREC) in Biglerville, Pennsylvania. According to the four established rules for pruning tall spindle trees, the first rule of removing branches based on the limb to trunk ratio, i.e., removal of branches greater than a certain diameter, can cover up to 70% of the pruning load (J. Schupp, Penn State University, personal communication, 16 Sept. 2019).

Five 'Fuji' trees were selected randomly, and 15 to 20 branches at different orientations were selected from each tree for the tests (the branches were cut multiple times at different locations and orientations). The diameter of each branch was recorded. The coordinates of the target locations as well as the angles of M1 and M2 were input manually to drive the linear actuators and the end-effector. Because the spatial requirement was the main consideration in this study, the angles of M1 and M2 were recorded for estimating the angular orientations and the workspace utilization of the end-effector. The pressure of the pneumatic cylinder was set at 800 to 825 kPa. In test 1, the 2.2 cm bore size pneumatic cylinder was used, and 100 cuts were performed as multiple cuts applied to one branch at different locations and diameters. In test 2, the 2.54 cm bore size pneumatic cylinder was used to provide greater cutting force, and 120 cuts were performed on randomly selected branches, including multiple cuts on one branch at different diameters and at different orientations on selected branches.

Results and Discussion

Torque Required for Cutting Branches

The relationship between the required cutting torque and the branch diameter is plotted in figure 7. A rational polynomial regression model was applied to the data to form the fitting curve, and the lower and upper bounds were also fitted. The data followed a rational 2×2 curve fit with an R^2 value of 0.9334. The results are helpful for selecting and optimizing the end-effector components, such as the pneumatic cylinder size and pressure, the orientation motor torque, and the mounting frame. The force sensor had the capacity to measure a maximum force of 2 kg; therefore, the test was conducted to cut branches with diameters ranging from 3 to 17 mm. Although the data are clustered around the trendline, a more sophisticated test, using a larger-capacity sensor, is necessary to extrapolate the data for larger-diameter branches with better accuracy. During the tests, it was observed that the required cutting force was greater for older branches than that for new branches. This factor was not considered when conducting the pruning force measurement tests, so further investigations are

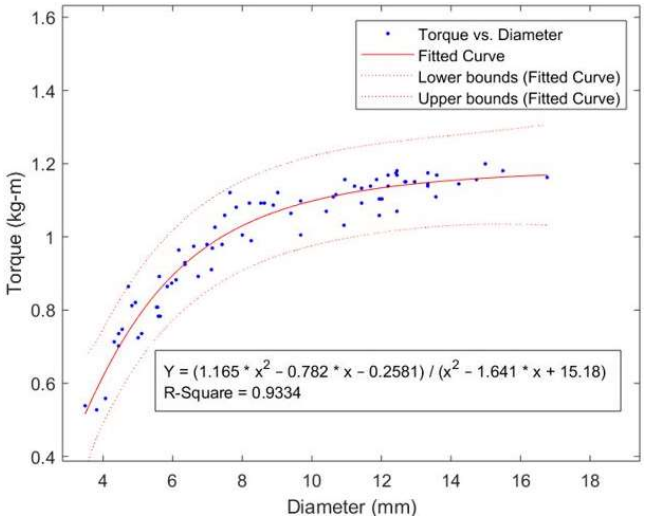

Figure 7. Torque required to prune branches of 'Fuji' apple trees.

required to establish a relationship for the difference in force required for cutting new and old branches. Different apple cultivars differ in the amount of force required to cut branches (J. Schupp, personal communication), and this also requires further evaluation.

Results of Workspace Simulation

The simulation results for the workspace and reachable points of the end-effector show the geometry of the mechanism with θ_1 and θ_2 both at 60° for better realization of obtaining the reachable points (fig. 8). Figures 8a and 8b show the reachable points in a given 3D space with step angles of 20° and 10°, respectively, for both θ_1 and θ_2. The end point tracking simulation shows that the end-effector was capable of maneuvering in a 3D workspace and has an indefinite number of reachable points in space. With the simultaneous rotation of both θ_1 and θ_2, the end-effector can maneuver in a 3D workspace, and based on the given dimensions, the workspace was a 26 cm diameter sphere, which allows the end-effector to operate in crowded apple tree canopies. Pruning a branch requires positioning the cutter perpendicular to the branch. For that purpose, the cutter frame orientation, which is illustrated with a single line in the direction of the cutter base, was drawn at a few simulated points (every 10th point at 20° steps for θ_1 and θ_2) and at all simulated points (at 10° steps for θ_1 and θ_2) in figures 8c and 8d, respectively. These cutter orientation lines show that the end-effector was capable of aligning the cutter in a wide range of possible orientations in the 3D workspace. Apple tree branches have a wide range of possible orientations, leading to little available space for maneuvering the end-effector. This simulation shows that the proposed end-effector can be aligned to all possible orientations while using a small workspace for maneuvering within the canopy.

Results of Field Experiment

For both field tests (test 1 and test 2), a total of 220 cuts were applied on selected branches at different positions and orientations. In test 1 (2.2 cm pneumatic cylinder), 65 of the 100 applied cuts were successful with a single stroke of the pneumatic cylinder (table 2). All branch diameters up to 8 mm were cut successfully. The pruner was able to make 20 successful cuts for branch diameters ranging from 8 to 10 mm with two strokes of the pneumatic cylinder. The 15 applied cuts on branch diameters greater than 10 mm were not successful even with two strokes of the pneumatic cylinder. In test 2 (2.54 cm pneumatic cylinder), the cutting capability of the pruner was improved. Of the 120 applied cuts, 90 were successful with a single stroke of the pneumatic cylinder, and all branch diameters up to 12 mm were cut successfully. Similarly, the pruner was able to make ten successful cuts on branch diameters ranging 12 to 14 mm with two strokes of the pneumatic cylinder. The developed end-effector was not able to cut branch diameters greater than 14 mm.

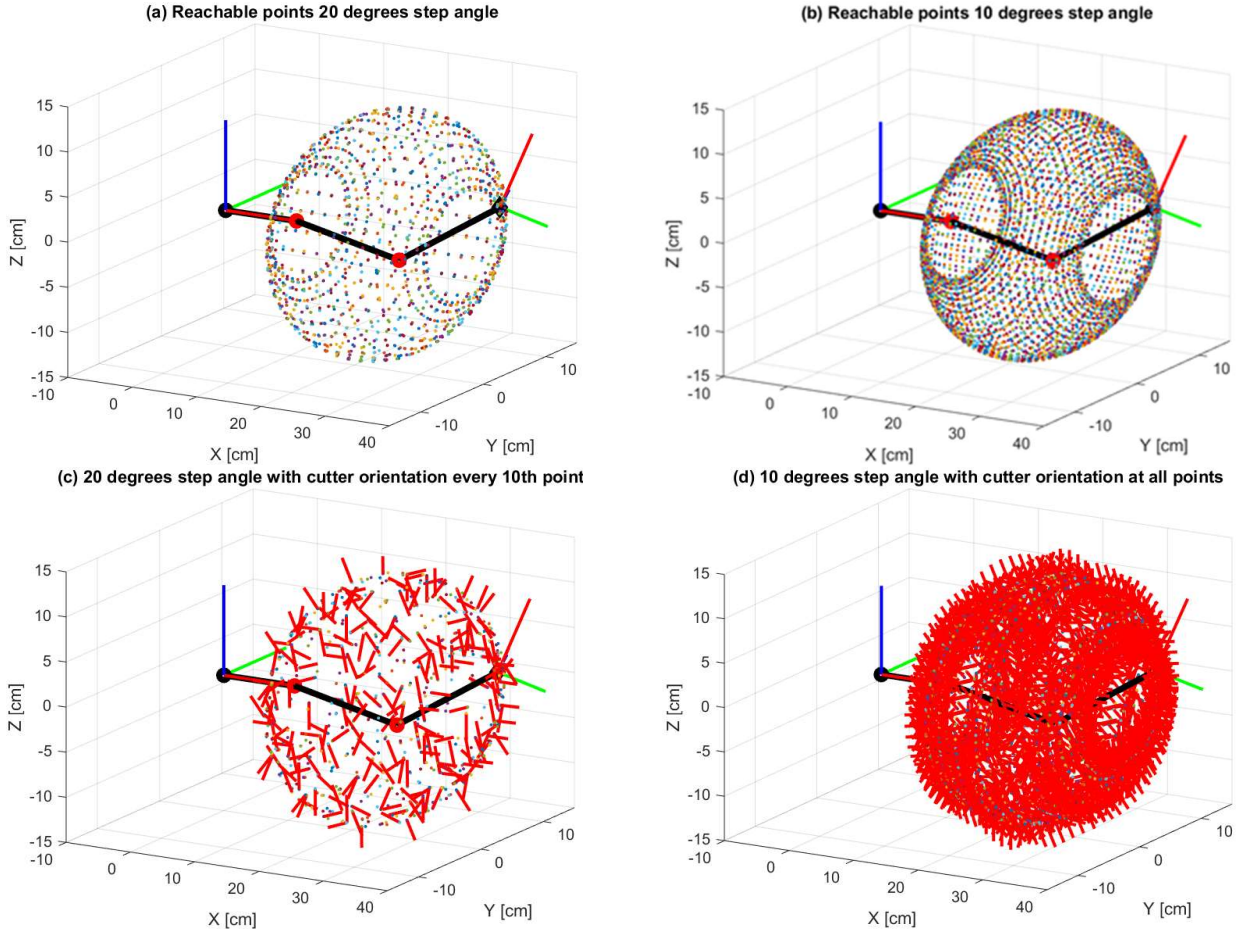

Figure 8. Simulation of reachable points and cutter orientations.

Table 2. Sample data for field tests of end-effector.

Test 1 (2.2 cm pneumatic cylinder)			Test 2 (2.54 cm pneumatic cylinder)		
Branch Diameter (mm)	M1 Angle (deg)	M2 Angle (deg)	Branch Diameter (mm)	M1 Angle (deg)	M2 Angle (deg)
4.15	00 [c]	90	6.75	00	35
5.25	00	90	6.00	-20	45
3.39	00	135	8.50	-45	60
4.66	00	70	7.25	-60	60
5.11	-30 [d]	45	6.10	-90	20
4.90	-75	45	9.75	10	00
5.15	-75	45	8.90	10	00
8.10 [a]	-60	45	8.81	-90	90
6.80	-60	20	9.84	-100	45
7.20	-75	20	10.11	-45	10
6.50	-115	20	10.60	00	-20
6.15	-75	20	12.20 [a]	00	-45
6.78	-75	20	4.20	45	-45
9.78 [b]	00	20	5.40	10	-45
7.55	00	45	7.65	-45	-60
3.00	00	70	14.06 [b]	-20	-90
3.33	25	90	10.01	-10	-100
3.41	45	90	10.20	-10	-100
4.07	25	00 [c]	6.80	-60	20
3.97	60	00	8.40	-60	10

[a] Maximum diameter of successful cut with single stroke.
[b] Unable to cut the branch with single stroke.
[c] M1 and M2 in-line with the arm is referred as 0.
[d] Negative sign indicates counterclockwise movement.

The rotation capability of the end-effector in two perpendicular directions (M1 and M2) gave it the ability to cut branches in a wide range of orientations in the 3D space. For any given target orientation, the end-effector produced smooth and split-free cuts on branches up to 8 and 12 mm diameter in test 1 and test 2, respectively.

The performance of the end-effector was found to be unsatisfactory for cutting branches with diameters greater than ~12 mm, as this task required two or three strokes of the pneumatic cylinder. The torque produced by the cutter was insufficient to produce enough force to cut these branches. A more powerful cutter is required to cut large-diameter branches, i.e., 12 mm and larger. For that purpose, the system may need to be equipped with a larger pneumatic cylinder or a modified electric pruner, considering the workspace utilization. Replacement of the pneumatic system with an electric pruner is expected to improve the cutter efficiency. It was also observed that placement of the target branch closer to the cutter pivot made it easier to cut, compared to when the target branch was closer to the tip of the blade. This was an important observation for developing an automatic trajectory and target positioning system.

Although the end-effector performed well for the objectives defined in this study, the designed system had low efficiency due to the manual positioning and aligning of the cutter with the target branches. It was also observed that the end-effector collided with branches, which may damage the system as well as the branches. Inverse kinematics and simulation of the integrated manipulator and end-effector are required to establish collision-free trajectories to reach targeted pruning locations. This simulation-generated collision-free tool path is expected to improve the efficiency of the system by automatically positioning and aligning the cutter. We also found that the forces required for cutting older branches (multi-year wood) were typically greater than those for young branches. Further investigations are required to establish a relationship between branch strength and age to develop a cutter powerful enough to prune older branches. Finally, to accurately reach the targeted branch, the effect of ground conditions will be taken into consideration using an inertial measurement unit (IMU) to provide real-time positioning of the robotic end-effector.

Most robotic pruning research has been performed on grapevines, and only a few studies have involved tree fruits (Gao and Lu, 2006; Kondo et al., 1993; Vision Robotics, 2015). Within the research on tree fruits, most studies have focused on branch identification and pruning location determination with machine vision systems, with few studies on the development of a pruning end-effector (Karkee et al., 2014; Medeiros et al., 2017; Tabb, 2009; Wang and Zhang, 2013). Botterill et al. (2017) developed mill-end cutter end-effector for pruning grapevines but did not consider the spatial requirements of the cutter, which limited its collision-free access to the canes. The results of the present study provide guidelines for designing an effective robotic end-effector for pruning fruit trees. The novelty of this study was its consideration of the spatial requirements for pruning using the flexibility of the end-effector, rather than a complex manipulator. The developed end-effector could maneuver at any orientation in a given 3D space, which helped to reduce the spatial requirements for a robotic system and improve access to targeted branches in a complex tree canopy.

CONCLUSIONS

In this study, a pruning end-effector was developed and integrated with a three-axis linear manipulator to perform pruning tasks on ‘Fuji’ apple trees. The branch cutting force was measured prior to the design of the robotic end-effector. A mathematical model was developed for simulation of the end-effector, followed by a series of field tests. The following conclusions can be drawn from the results:

- The branch cutting force had a rational 2×2 curve fit relationship with the branch diameter, with an R^2 value of 0.93. Less torque was required for pruning younger branches than older branches of the same diameter. Further investigations are required to establish a relationship between branch strength and age.
- The endpoint tracking simulation suggested that the designed end-effector can be aligned in a wide range of orientations. The end-effector can maneuver in a spherical workspace with a diameter of 26 cm to align itself to any given orientation.
- The end-effector cut branches up to 12 mm in diameter with the 2.54 cm pneumatic cylinder at a pressure of 800 to 825 kPa. With this capability, it can be used for robotic pruning in modern apple tree architectures. The cutting capability could be improved with increased cylinder size and pressure.
- The cutter of the end-effector was maneuvered to align perpendicularly with the target branches before cutting was applied, and the test results indicated that the end-effector can cut branches in a wide range of

orientations. The wide range of alignments and the compact size of the end-effector permit its application for robotic pruning in complex apple tree architectures.

Future studies will be conducted on the design optimization of the end-effector to minimize its workspace utilization, especially where branches are crowded and overlapped. To improve the efficiency, studies will be conducted to develop a 3 rotational DoF end-effector using an electric shear blade pruner. Further studies will also be conducted to simulate the accessibility of a random branch in a complex tree canopy to the integrated end-effector and manipulator. An automatic control system and vision system will be integrated for moving the end-effector from one branch to another while following a collision-free trajectory.

Acknowledgements

This research was partially supported by USDA NIFA Federal Appropriations under Project PEN04547 and Accession No. 1001036. We would like to give special thanks for the support from the Penn State College of Agricultural Sciences Stoy G. and Della E. Sunday program and Northeast Sustainable Agriculture Research and Education (SARE) Graduate Student Grant GNE19-225-33243.

References

Bac, C. W., van Henten, E. J., Hemming, J., & Edan, Y. (2014). Harvesting robots for high-value crops: State-of-the-art review and challenges ahead. *J. Field Robot., 31*(6), 888-911. https://doi.org/10.1002/rob.21525

Botterill, T., Paulin, S., Green, R., Williams, S., Lin, J., Saxton, V., ... Corbett-Davies, S. (2017). A robot system for pruning grapevines. *J. Field Robot., 34*(6), 1100-1122. https://doi.org/10.1002/rob.21680

Dong, G., & Zhu, Z. H. (2015). Position-based visual servo control of autonomous robotic manipulators. *Acta Astronaut., 115*, 291-302. https://doi.org/10.1016/j.actaastro.2015.05.036

Feng, Q., Zou, W., Fan, P., Zhang, C., & Wang, X. (2018). Design and test of robotic harvesting system for cherry tomato. *Intl. J. Agric. Biol. Eng., 11*(1), 96-100. https://doi.org/10.25165/j.ijabe.20181101.2853

Gallardo, K., Taylor, M., & Hinman, H. (2010). 2009 Cost estimates of establishing and producing Gala apples in Washington. Pullman, WA: Washington State University Extension. Retrieved from http://ses.wsu.edu/wp-content/uploads/2018/10/FS041E.pdf

Gao, M., & Lu, T. (2006). Image processing and analysis for autonomous grapevine pruning. *Proc. Intl. Conf. on Mechatronics and Automation* (pp. 922-927). Piscataway, NJ: IEEE. https://doi.org/10.1109/ICMA.2006.257748

Glenn, D. M., & Campostrini, E. (2011). Girdling and summer pruning in apple increase soil respiration. *Scientia Hort., 129*(4), 889-893. https://doi.org/10.1016/j.scienta.2011.04.023

He, L., & Schupp, J. (2018). Sensing and automation in pruning of apple trees: A review. *Agron., 8*(10), 211. https://doi.org/10.3390/agronomy8100211

Huang, B., Shao, M., & Chen, W. (2016). Design and research on end effector of a pruning robot. *Intl. J. Simulation Syst. Sci. Tech., 17*(36).

Hui, Y., Liu, H., Zhang, H., Wu, Y., Li, Y., Fu, Z., & Wang, D. (2018). Design and experiment of end-effector for eggplant picking robot. ASABE Paper No. 1800387. St. Joseph, MI: ASABE. https://doi.org/10.13031/aim.201800387

Jeon, H. Y., & Tian, L. F. (2009). Direct application end effector for a precise weed control robot. *Biosyst. Eng., 104*(4), 458-464. https://doi.org/10.1016/j.biosystemseng.2009.09.005

Kapach, K., Barnea, E., Mairon, R., Edan, Y., & Ben-Shahar, O. (2012). Computer vision for fruit harvesting robots: State of the art and challenges ahead. *Intl. J. Comput. Vision Robot, 3*(1-2), 4-34. https://doi.org/10.1504/IJCVR.2012.046419

Karkee, M., Adhikari, B., Amatya, S., & Zhang, Q. (2014). Identification of pruning branches in tall spindle apple trees for automated pruning. *Comput. Electron. Agric., 103*, 127-135. https://doi.org/10.1016/j.compag.2014.02.013

Kondo, N., & Ting, K. C. (1998). Robotics for plant production. *Artif. Intel. Rev., 12*(1-3), 227-243. https://doi.org/10.1007/978-94-011-5048-4_12

Kondo, N., Shibano, Y., Mohri, K., & Monta, M. (1994). Basic studies on robot to work in vineyard (Part 2). *J. Japanese Soc. Agric. Mach., 56*(1), 45-53.

Kondo, N., Shibano, Y., Mohri, K., Monta, M., & Okamura, S. (1993). Basic studies on robot to work in vineyard (Part 1). *J. Japanese Soc. Agric. Mach., 55*(6), 85-94.

Lehnert, R. (2012). Robotic pruning. *Good Fruit Grower* (1 Nov. 2012). Retrieved from https://www.goodfruit.com/robotic-pruning/

Li, P., Lee, S.-H., & Hsu, H.-Y. (2011). Review on fruit harvesting method for potential use of automatic fruit harvesting systems. *Procedia Eng., 23*, 351-366. https://doi.org/10.1016/j.proeng.2011.11.2514

Lindner, M., Kolb, A., & Hartmann, K. (2007). Data-fusion of PMD-based distance information and high-resolution RGB images. *Proc. Intl. Symp. on Signals, Circuits and Systems*. Piscataway, NJ: IEEE. https://doi.org/10.1109/ISSCS.2007.4292666

Ling, P. P., Ehsani, R., Ting, K. C., Chi, Y.-T., Ramalingam, N., Klingman, M. H., & Draper, C. (2004). Sensing and end-effector for a robotic tomato harvester. ASAE Paper No. 043088. St. Joseph, MI: ASAE. https://doi.org/10.13031/2013.16727

Medeiros, H., Kim, D., Sun, J., Seshadri, H., Akbar, S. A., Elfiky, N. M., & Park, J. (2017). Modeling dormant fruit trees for agricultural automation. *J. Field Robot., 34*(7), 1203-1224. https://doi.org/10.1002/rob.21679

Mercier, V., Bussi, C., Plenet, D., & Lescourret, F. (2008). Effects of limiting irrigation and of manual pruning on brown rot incidence in peach. *Crop Prot., 27*(3-5), 678-688. https://doi.org/10.1016/j.cropro.2007.09.013

Mika, A., Buler, Z., & Treder, W. (2016). Mechanical pruning of apple trees as an alternative to manual pruning. *Acta Sci. Pol. Hortorum Cultus, 15*(1), 113-121.

Nakarmi, A. D., & Tang, L. (2012). Automatic inter-plant spacing sensing at early growth stages using a 3D vision sensor. *Comput. Electron. Agric., 82*, 23-31. https://doi.org/10.1016/j.compag.2011.12.011

Silwal, A. (2016). Machine vision system for robotic apple harvesting in fruiting wall orchards. PhD diss. Pullman, WA: Washington State University, Department of Biological Systems Engineering.

Spong, M. W., Hutchinson, S., & Vidyasagar, M. (2006). *Robot dynamics and controls*. New York, NY: Wiley. Retrieved from https://doi.org/10.1201/9781420037043

Tabb, A. (2009). Three-dimensional reconstruction of fruit trees by a shape from silhouette method. ASABE Paper No. 096138. St. Joseph, MI: ASABE. https://doi.org/10.13031/2013.27064

USDA-NASS. (2018). Noncitrus fruits and nuts: 2017 summary. Washington, DC: USDA National Agricultural Statistics Service. Retrieved from

https://usda.mannlib.cornell.edu/usda/current/NoncFruiNu/NoncFruiNu-06-26-2018.pdf
Vision Robotics. (2015). Intelligent autonomous grapevine pruner. San Diego, CA: Vision Robotics Corp. Retrieved from https://www.visionrobotics.com/vr-grapevine-pruner
Wang, Q., & Zhang, Q. (2013). Three-dimensional reconstruction of a dormant tree using RGB-D cameras. ASABE Paper No. 131593521. St. Joseph, MI: ASABE. https://doi.org/http://dx.doi.org/10.13031/aim.20131593521
Zhang, D., Lv, J., Wei, J., Zhang, Y., & Cheng, Y. (2011). Design and control of an apple harvesting robot. *Biosyst. Eng., 110*(2), 112-122. https://doi.org/10.1016/j.biosystemseng.2011.07.005
Zhao, Y., Gong, L., Liu, C., & Huang, Y. (2016). Dual-arm robot design and testing for harvesting tomato in greenhouse. *IFAC-PapersOnLine, 49*(16), 161-165. https://doi.org/10.1016/j.ifacol.2016.10.030